Dissipationless spin-valley current in zigzag-edge graphene ribbons with a net magnetization

Kyu Won Lee and Cheol Eui Lee*
Department of Physics, Korea University, Seoul 02841, Korea
(Received 19 January 2017; revised manuscript received 20 March 2017; published 16 May 2017)

We have investigated the spin-valley degree of freedom characterized by the product of spin and valley indices in zigzag-edge graphene ribbons with a net magnetization by using a tight-binding model. We found that the CT invariance leads to the spin-valley current which is neither spin polarized nor valley polarized but fully spin-valley polarized, where C and T are the charge conjugation and the time-reversal operation, respectively. In the quantum Hall regime, the gapless edge states protected by the CPT invariance carry the spin-valley degree of freedom leading to a dissipationless spin-valley current, where P is the inversion operation.

DOI: 10.1103/PhysRevB.95.195132

I. INTRODUCTION

In recent years, a great deal of attention has been paid to the spin-valley coupling, which is expected to lead to fully polarized spin and valley currents essential in spintronics and valleytronics [1–6]. However, although the coupled spin-valley characterized by the product of spin and valley indices is also a new degree of freedom other than spin and valley, spin-valley coupling has been investigated as a route to spin and valley currents but little attention has been paid to the spin-valley current itself, which enables electronics based on the spin-valley degree of freedom. Here, we show that zigzag-edge graphene ribbons with a net magnetization whether spontaneous or induced can generate dissipationless spin-valley current, which is neither spin polarized nor valley polarized but fully spin-valley polarized. A scheme of a spin-valley valve which can generate and detect spin-valley current is suggested. Our paper is believed to contribute to the spin-valley physics and an advanced electronics based on the spin-valley degree of freedom.

In addition to the charge and spin degree of freedom, electrons in a honeycomb lattice can have a valley degree of freedom corresponding to the corners (K and K') of the first Brillouin zone, which can be coupled to other degrees of freedom [7]. Inversion symmetry breaking due to a staggered sublattice potential or an antiferromagnetic order can remove the valley degeneracy and can give rise to the valley Hall effect where carriers in different valleys flow to opposite transverse edges [6–8]. In monolayer transition-metal dichalcogenides with a broken inversion symmetry, which is described by the massive Dirac fermions, the spin splitting of the valence bands arising from intrinsic spin-orbit interaction is opposite at the two valleys due to a time-reversal symmetry [1–3]. The spin-valley coupling was predicted to lead to strongly suppressed spin and valley relaxations at the valence-band edge and to induce a valley Hall effect with a spin Hall effect [3]. In graphene and silecene, a spin-orbit interaction and a staggered sublattice potential also were reported to result in spin- and valley-dependent band gaps [5,9,10], and a (pseudo)magnetic field induced by magnetization or strain as well as photoirradiation were suggested as a way to fully polarized spin and valley current generation [5,11].

The spin-valley degree of freedom determines the relative orientation between the spin and the valley and can have two states just like the spin and the valley. In bilayer graphene, electron-electron interaction was predicted to enable the quantum spin-valley Hall state where carriers with opposite spin-valley indices flow to opposite transverse edges [12]. In zigzag-edge graphene nanoribbons (ZGNRs), a staggered sublattice potential along with magnetization at the edge atoms were predicted to induce spin- and valley-polarized gapless edge states [13]. In the same work, spin-valley current can be found in the ferromagnetic edge state of the ZGNR, although the authors did not pay attention to the spin-valley degree of freedom [13].

A ZGNR has flat bands at the Fermi level (E_F) corresponding to the edge-localized electrons, whose electron-electron interaction has been known to lead to an antiferromagnetic edge state for narrow ribbons and to a ferromagnetic edge state for wide ribbons [14–16]. Ferromagnetic graphene under a magnetic field was predicted to be a quantum spin Hall (QSH) insulator, which can be responsible for the quantum Hall conductance plateau at the filling factor of $\nu = 0$ [17]. The electron-electron interaction and the electron-phonon interaction in graphene can remove the valley degeneracy of the Landau level, which can be responsible for the quantum Hall conductance plateau at $\nu = \pm 1$ [18,19]. Thus, gapless edge states with a spin-valley coupling can be expected in a ZGNR with an electron-electron interaction under a magnetic field even in the absence of a spin-orbit coupling.

In this paper using a tight-binding (TB) model, we show that spin-valley current arises from invariance of the band structure regardless of gapless edge states and origin of magnetization and that spin-valley current can be generated and detected by using an external magnetic field. We call for renewed attention to the band structure of a ZGNR with a net magnetization spontaneous or induced, which has band crossings at E_F between the two bands with opposite spin orientations. We also call for attention to the spin orientations of the crossing bands which are reversed at opposite valleys [20,21] as shown in Fig. 1. We identify that due to the CT invariance the edge states with the same spin-valley index propagate in the same direction generating a spin-valley current which is neither spin polarized nor valley polarized but fully spin-valley polarized. C and T

*rscel@korea.ac.kr

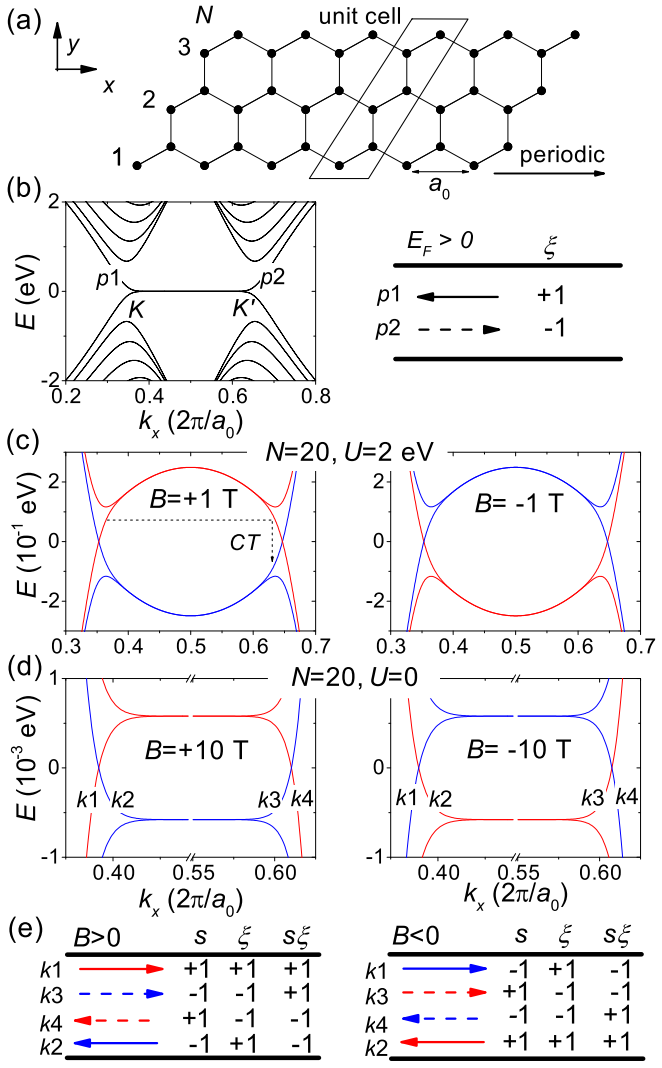

FIG. 1. Spin-valley current. (a) Atomic geometry of 3-ZGNR. (b) Band structure of 20-ZGNR when $B = U = 0$ (left) and a schematic of the propagating states at $E_F > 0$ where the arrows indicate the propagating direction. $p1$ and $p2$ indicate the dispersion curve corresponding to the propagating states. (c) Band structures of 20-ZGNR in the ferromagnetic state for $U = 2$ eV and $B = \pm 1$ T where the left and right sides correspond to the opposite magnetizations. (d) Band structures of 20-ZGNR for $U = 0$ and $B = \pm 10$ T where the left and right sides correspond to the opposite magnetization. The Zeeman energy $E_z = \mu_B B$ is equal to 0.58 meV for $B = 10$ T. (e) Schematics for the propagating states at $E_F = 0$. The solid and dashed arrows correspond to the opposite valleys ($\xi = \pm 1$). The red and blue colors correspond to the opposite spins ($s = \pm 1$). $s\xi = \pm 1$ corresponds to the coupled spin-valley index. In panels (d) and (e), $k1$–$k4$ indicate the dispersion curve corresponding to the propagating states.

are the charge conjugation and the time-reversal operations, respectively. In the quantum Hall regime, the gapless edge states protected by the CPT invariance carry the spin-valley degree of freedom leading to a dissipationless spin-valley current, where P is the inversion operation. Since the band crossings also are found in the multilayer ZGNRs with a net magnetization, a spin-valley current can be expected even in graphite ribbons.

II. METHODS

In this paper, the ZGNR was considered as a one-dimensional system periodic on the x axis (zigzag direction) with a lattice constant of $a_0 = 2.46$ Å as shown in Fig. 1(a) and will be referred to as N-ZGNR, where N is the number of C-C pairs in a unit cell. The TB Hamiltonian can be given as follows [21]:

$$H = -\sum_{\langle p,q\rangle s} \gamma_{pq} c^{\dagger}_{ps} c_{qs} + U \sum_{ps} \left(\langle n_{ps'} \rangle - \frac{1}{2} \right) n_{ps} + \mu_B B \sum_{ps} s n_{ps} + \sum_{ps} \delta_p n_{ps} + \text{H.c.}, \quad (1)$$

where c_{ps} is the electron annihilation operator at a site p with a spin $s = \pm 1$ ($= -s'$) and $n_{ps} = c^{\dagger}_{ps} c_{ps}$. $\gamma_{pq} = \gamma_0 e^{i(e/\hbar)\phi_{pq}}$ with the nearest-neighbor hopping energy of $\gamma_0 = 2.7$ eV and the magnetic flux ϕ_{pq}, which is calculated using the Peierls substitution $\phi_{pq} = \int_{\vec{r}_p}^{\vec{r}_q} \vec{A} \cdot d\vec{r}$ with $\vec{A}$ being the vector potential according to previous works [22]. We use the Landau gauge $\vec{A} = (-By, 0, 0)$ with a magnetic-field $\vec{B} = B\hat{z}$. U is the on-site Coulomb repulsion energy. The staggered AB-sublattice potential δ_p is $+\delta$ for sublattice A and $-\delta$ for sublattice B. The third term describes the Zeeman splitting with a Bohr magneton μ_B. The second term corresponding to the mean-field-approximated Hubbard Hamiltonian at half-filling describes the on-site electron-electron interaction. $\langle n_{ps} \rangle$ is the electron density for spin-up and spin-down electrons at a site p, which should be calculated in a self-consistent way. $U = 0$ for a paramagnetic state and $U = 2$ eV for a ferromagnetic edge state were used [23]. The TB model was self-consistently solved for N-ZGNR by using a PYTHTB code [24], and the transmittance between the two leads separated by a scattering region shown in Fig. 2 was calculated by using a KWANT code [25].

III. RESULTS AND DISCUSSION

Figure 1(b) shows the band structure of 20-ZGNR in the paramagnetic state when $B = U = 0$ (left side), which shows the flat bands corresponding to the edge-localized electrons at $E_F = 0$, in agreement with previous works [26]. Although the flat bands do not contribute to charge transport at $E_F = 0$, the band velocity at the opposite valley has opposite signs at $E_F \neq 0$, indicating that the charge transport at $E_F \neq 0$ is valley polarized as shown on the right-hand side of Fig. 1(b) [27]. $p1$ and $p2$ indicate the dispersion curves corresponding to the propagating states. Figure 1(c) shows the band structures of 20-ZGNR in the ferromagnetic edge state with $U = 2$ eV. The orientation of the spontaneous magnetization was reversed by applying the magnetic-field $B = \pm 1$ T. Figure 1(d) shows the band structures of 20-ZGNR in the paramagnetic state with $U = 0$ and $B = \pm 10$ T. The orientation of the induced magnetization was reversed by the magnetic field. The band structures on the left and right sides of Figs. 1(c) and 1(d) correspond to the opposite orientations of the magnetization. The Zeeman energy $E_z = \mu_B B$ (half the Zeeman splitting) is equal to 0.58 meV for $B = 10$ T.

As shown in Figs. 1(c) and 1(d), the magnetization spontaneous or induced removes the spin degeneracy of the

(a)

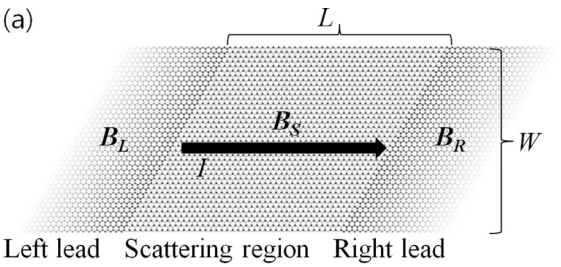

(b) E_F=E_Z/2, W=17 nm, L=118 nm, B=10 T

B_L	B_S	B_R	σ_L	(s,ξ)	$s\xi$	
0	0	0	2	(+1,+1) (-1,+1)	0	ξ-filter
+	+	+	2	(+1,+1) (-1,-1)	+1	$s\xi$-valve
+	+	-	0			
+	-	+	0			
+	0	+	1	(+1,+1)	+1	ξ-filtering $s\xi$-valve
+	0	-	0			
0	+	0	1	(+1,+1)	+1	s,ξ-filter
0	+	+	1	(+1,+1)	+1	ξ-filtering $s\xi$-valve
0	+	-	0			

FIG. 2. Spin-valley valve. (a) Scheme of spin-valley valve where ZGNR is divided into left and right leads and scattering region of length L and width W, each of which has a magnetic-field B_L, B_R, and B_S perpendicular to the layer. (b) Two-terminal conductance σ_L in units of e^2/h obtained by calculating the transmittance from the left lead to the right lead with $U = 0$, $E_F = E_Z/2$, $W = 17$ nm ($N = 80$), $L = 118$ nm, and $B = 10$ T, where $E_Z = 0.58$ meV is the Zeeman energy. B_L, B_R, and B_S can have 0 and $\pm B$. (s,ξ) indicates the spin and valley indices of the transmitting modes.

flat bands, which undergo energy-level shifts of opposite signs for opposite spins leading to band crossings at $E_F = 0$ between the two bands of opposite spin polarizations. The spin polarizations of the crossing bands are opposite at the two valleys, and reversal of the magnetization reverses the spin polarizations of the crossing bands. In Fig. 1(d), $k1$–$k4$ indicate the dispersion curves resulting from the spin splitting of the flat bands and corresponding to the charge transport at E_F. For example, the dispersion curves $k2$ and $k3$, respectively, come from the dispersion curves $p1$ and $p2$ indicated in Fig. 1(b).

From the band velocity at $E_F = 0$, we can construct a schematic for the propagating states as shown in Fig. 1(e). In Fig. 1(d), $k1$–$k4$ indicate the dispersion curves corresponding to the propagating states in Fig. 1(e). The right and left arrows indicate the opposite propagating directions. The solid and dashed arrows correspond to the opposite valleys ($\xi = \pm 1$). The red and blue colors correspond to the opposite spins ($s = \pm 1$), and $s\xi = \pm 1$ corresponds to the coupled spin-valley index. On the left side ($B > 0$) of Fig. 1(e), let us note the two states propagating in the positive direction. The two states have the opposite s and the opposite ξ but the same $s\xi$, leading to the spin-valley current which is neither spin polarized nor valley polarized but fully spin-valley polarized. Reversal of the magnetization ($B < 0$) as shown on the right side of Fig. 1(e) reverses $s\xi$ of the spin-valley current. It should be noted that the two states propagating in a given direction with the same $s\xi$ are the CT partners of each other. $CT|E,k,s,v_B\rangle = |-E,-k,-s,v_B\rangle$ as shown in Fig. 1(c) where the band velocity $v_B = \frac{1}{\hbar}\frac{dE}{dk}$. The CT partners have the same $s\xi$ since the CT operation simultaneously reverses the spin and valley indices and propagate in the same direction, indicating that the spin-valley current is due to the CT invariance.

As discussed above, a ZGNR with a net magnetization can generate a spin-valley current, whose spin-valley index can be reversed by using the magnetic field. Thus, a scheme of the spin-valley valve generating and detecting the spin-valley current can be suggested as shown in Fig. 2(a) where the ZGNR is divided into the left and right leads and scattering region of length L and width W, each of which has a magnetic-field B_L, B_R, and B_S perpendicular to the layer. Figure 2(b) shows the two-terminal conductance σ_L in units of e^2/h, obtained by calculating the transmittance from the left lead to the right lead with $U = 0$, $E_F = E_Z/2$, $W = 17$, $L = 118$ nm, and $B = 10$ T, where $E_Z = 0.58$ meV. B_L, B_R, and B_S can have 0 and $\pm B$. E_F was chosen to be $0 < E_F < E_Z$. Since the ZGNR is a valley filter when $B = 0$ and is a spin-valley filter when $B \neq 0$, combinations of (B_L, B_S, and B_R) can lead to various functions.

For example, when $(B_L, B_S, B_R) = (+B, 0, \pm B)$, which can be achieved by using two ferromagnetic electrodes, two $s\xi = +1$ (spin-valley-polarized) states with $(s,\xi) = (+1,+1)$ and $(-1,-1)$ propagate from the left lead to the scattering region. Only a $\xi = +1$ (valley-polarized) state with $(s,\xi) = (+1,+1)$ can pass the scattering region. The $(+1,+1)$ state with $s\xi = +1$ can propagate into the right lead when $B_R = +B$ but cannot when $B_R = -B$. The valley-filtering spin-valley valve is also a spin and a valley valve. Because the spin-valley current arises from the CT invariant band structure regardless of the origin of the magnetization, we can readily expect similar valve effects in the ferromagnetic state with a finite U by using a magnetic field. Multilayer ZGNRs have essentially the same band structure as that of the ZGNR except that the number of states at E_F increases with the number of layers and thus even the zigzag-edge graphite ribbons can be used for the spin-valley current. For a valve effect to be observed in experiments, polarized carriers should travel to the detector without losing their polarization. In fact, spin- and valley-relaxation lengths in graphene were reported to be longer than ~ 1 μm in experiments on spin and valley currents [28,29]. Thus, we may expect that a spin-valley valve can be realized in real experiments by using a device similar to the one used for a spin valve [28], even if an abrupt change in the magnetic field at the scale of one atom is not possible.

Next, we will discuss the spin-valley degree of freedom in the quantum Hall regime in the presence and absence of electron-electron interactions. Whereas the crossing bands correspond to the edge states, the electron density at the band crossing point is distributed equally on both edges for narrow ribbons under a low magnetic field, and any quantum Hall effect cannot be expected. For wide ribbons under a high magnetic field, the electron density of the spin- and valley-resolved states at $E_F = 0$ are concentrated on an edge

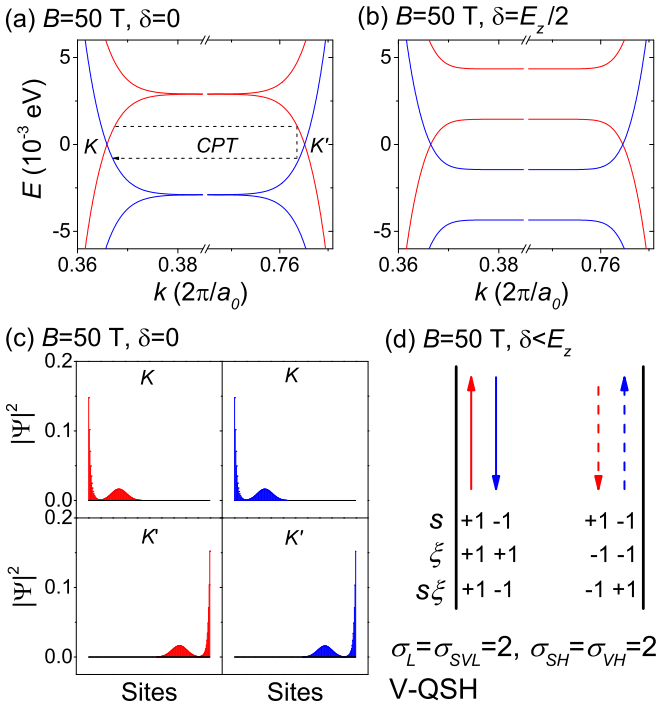

FIG. 3. Quantum Hall state for $U = 0$. 200-ZGNR in the paramagnetic state under $B = 50$ T. E_z is equal to 2.89 meV for $B = 50$ T. Band structures when (a) $\delta = 0$ and (b) $\delta = E_Z/2$. (c) $|\Psi|^2$ at $E_F = 0$ for $\delta = 0$. (d) Schematic for the propagating states at $E_F = 0$ constructed from panels (a)–(c). σ_{SVL}, σ_{SH}, and σ_{VH} are the two-terminal spin-valley conductance, the spin Hall conductance, and the valley Hall conductance, respectively. The same conventions as in Fig. 1 are used.

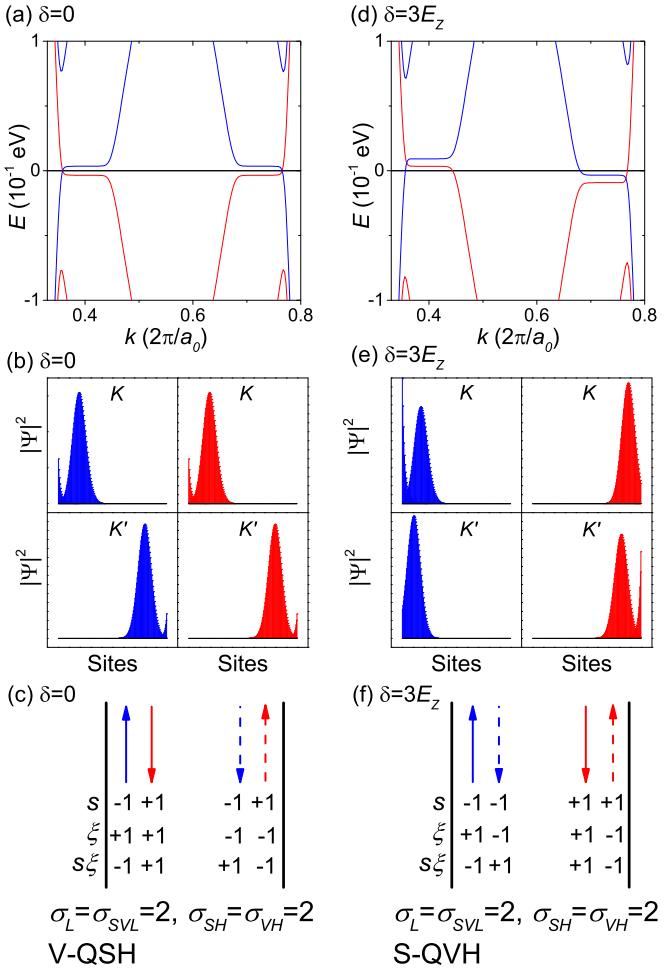

FIG. 4. Quantum Hall state for $U = 2$ eV. A 200-ZGNR in the ferromagnetic edge state under $B = 50$ T. Band structures when (a) $\delta = 0$ and (d) $\delta = 3E_Z$. $|\Psi|^2$ at $E_F = 0$ when (b) $\delta = 0$ and (e) $\delta = 3E_Z$. Schematics for the propagating states when (c) $\delta = 0$ and (f) $\delta = 3E_Z$. The same conventions as in Fig. 3 are used.

as shown in Fig. 3(c), indicating a possible quantum Hall effect. Figure 3 shows the quantum Hall regime of 200-ZGNR in the paramagnetic state ($U = 0$) under $B = 50$ T, where $E_Z = 2.89$ meV. Under a staggered potential $\delta < E_Z$, the band crossings are preserved as shown in Figs. 3(a) and 3(b). When $\delta > E_Z$, the ZGNR becomes an ordinary insulator with a band gap.

From v_B and $|\Psi|^2$ at $E_F = 0$ shown in Figs. 3(a)–3(c), we can construct a schematic for propagating states in the quantum Hall regime as shown in Fig. 3(d). Since each state contributes e^2/h to the conductance, the (Hall) conductance can be estimated in units of e^2/h by counting the number of the spin-, valley-, and edge-resolved states propagating in a given direction. σ_{SVL}, σ_{SH}, and σ_{VH} are the two-terminal spin-valley conductance, the spin Hall conductance, and the valley Hall conductance, respectively. When $\delta < E_Z$, $\sigma_L = \sigma_{SVL} = 2$ indicates fully spin-valley-polarized current neither spin polarized nor valley polarized, and $\sigma_{SH} = \sigma_{VH} = 2$ indicates the coexisting quantum valley Hall (QVH) and QSH effects. Despite the QVH conductance, this state is different from the well-known QVH state where two opposite valley channels propagate in the opposite directions at a given edge [30,31].

The state can be referred to as the valley-polarized QSH (V-QSH) state with valley-polarized edges of opposite signs since reversal of the propagating direction should accompany a spin flip and backscattering is forbidden in the absence of a spin-flip scattering. The V-QSH state is also different from the well-known QSH state originating from the spin-orbit interaction and is protected by the time-reversal symmetry which is broken under a magnetic field [32]. In the V-QSH state, the two counterpropagating states at a given edge (see Fig. 3) are the CPT partners of each other, indicating that the gapless edge states are protected by the CPT invariance and the spin-valley current becomes dissipationless since the spin-valley degree of freedom is carried by the gapless edge states. The CPT partners have the same valley index $CPT|E,k,s,v_B\rangle = |-E,k,-s,-v_B\rangle$ as shown in Fig. 3(a), leading to the valley-polarized edges of opposite signs. The CT-invariant QSH state already was predicted in ferromagnetic graphene without considering the valley degree of freedom [17]. Since the quantum (charge) Hall conductance is zero, the V-QSH state corresponds to the $\nu = 0$ quantum Hall state.

Figures 4(a)–4(c) show the quantum Hall regime of 200-ZGNR in the ferromagnetic edge state when $U = 2$ eV, $B = 50$ T, and $\delta = 0$. Figure 4(a) shows the band structure where the spin splitting of the $n = 0$ Landau level is larger than $2E_Z$ due to the electron-electron interaction and the band

structure shows CT and CPT invariances. Figure 4(b) shows $|\Psi|^2$ at $E_F = 0$, indicating that the opposite edges have the opposite valley indices. Figure 4(c) shows a schematic for the propagating states at $E_F = 0$, which shows the same V-QSH state protected by the CPT invariance and the dissipationless spin-valley current due to the CT invariance as in the case of $U = 0$ shown in Fig. 3. The V-QSH state persists when $\delta < 1.6E_Z$.

Figures 4(d)–4(f) show the quantum Hall regime of 200-ZGNR in the ferromagnetic edge state when $U = 2$ eV, $B = 50$ T, and $\delta = 3E_Z$. Figure 4(d) shows the band structure of 200-ZGNR. Contrasting to the case of $U = 0$ shown in Fig. 3, the staggered potential larger than the spin splitting of the $n = 0$ Landau level ($\delta > 1.6E_Z$) does not open a band gap. Instead, the staggered potential induces $n = 0$ Landau-level shifts of opposite signs at the opposite valleys, removing the valley degeneracy and only preserving the CT invariance. Figure 4(e) shows $|\Psi|^2$ at $E_F = 0$, indicating that the opposite edges have the opposite spins. Figure 4(f) shows a schematic for the propagating states at $E_F = 0$, where $\sigma_L = \sigma_{SVL} = 2$ indicates fully spin-valley-polarized current due to the CT invariance and $\sigma_{SH} = \sigma_{VH} = 2$ indicates the coexisting QSH and QVH effects. Despite the QSH conductance, this state is different from the well-known QSH state where two opposite spin channels propagate in the opposite directions at a given edge [32]. The state can be referred to as the spin-polarized QVH (S-QVH) state with spin-polarized edges of the opposite signs since the reversal of the propagating direction should accompany a valley flip and backscattering is forbidden by the K-K' separation in the Brillouin zone. Due to the lack of the CPT invariance in the edge state bands, the QSH state can no longer be protected. Since the quantum (charge) Hall conductance is zero, the S-QVH state corresponds to the $\nu = 0$ quantum Hall state.

To summarize, we have investigated the spin-valley degree of freedom in zigzag-edge graphene nanoribbons with a net magnetization by using the tight-binding model where the CT invariance was found to lead to a spin-valley current neither spin polarized nor valley polarized but fully spin-valley polarized. In the quantum Hall regime, the gapless edge states protected by the CPT invariance carry the spin-valley degree of freedom, leading to a dissipationless spin-valley current. Since the spin-valley polarization can be reversed by using a magnetic field, a scheme of the spin-valley valve can be suggested for an advanced electronics based on the spin-valley degree of freedom.

ACKNOWLEDGMENTS

This work was supported by the National Research Foundation of Korea (Projects No. 2016R1D1A1A09917003, No. 2016R1D1A1B03931144, No. 2015M1A7A1A01002234, and No. NRF-2010-0027963). K.W.L. gratefully acknowledges a Korea University research grant.

[1] Y. Saito, Y. Nakamura, M. S. Bahramy, Y. Kohama, J. Ye, Y. Kasahara, Y. Nakagawa, M. Onga, M. Tokunaga, T. Nojima, Y. Yanase, and Y. Iwasa, Nat. Phys. **12**, 144 (2016).
[2] X. Xu, W. Yao, D. Xiao, and T. F. Heinz, Nat. Phys. **10**, 343 (2014).
[3] D. Xiao, G.-B. Liu, W. Feng, X. Xu, and W. Yao, Phys. Rev. Lett. **108**, 196802 (2012).
[4] Q.-P. Wu, Z.-F. Liu, A.-X. Chen, X.-B. Xiao, and Z.-M. Liu, Sci. Rep. **6**, 21590 (2016).
[5] M. M. Grujić, M. Ž Tadić, and F. M. Peeters, Phys. Rev. Lett. **113**, 046601 (2014).
[6] J. Wang, M. Long, W.-S. Zhao, Y. Hu, G. Wang, and K. S. Chan, J. Phys.: Condens. Matter **28**, 285302 (2016).
[7] D. Xiao, W. Yao, and Q. Niu, Phys. Rev. Lett. **99**, 236809 (2007).
[8] X. Li, T. Cao, Q. Niu, J. Shi, and J. Feng, Proc. Natl. Acad. Sci. USA **110**, 3738 (2013).
[9] M. Ezawa, Phys. Rev. Lett. **109**, 055502 (2012).
[10] T. Yokoyama, Phys. Rev. B **87**, 241409(R) (2013).
[11] M. Ezawa, Phys. Rev. Lett. **110**, 026603 (2013).
[12] F. Zhang, J. Jung, G. A. Fiete, Q. Niu, and A. H. MacDonald, Phys. Rev. Lett. **106**, 156801 (2011).
[13] Z. Qiao, S. A. Yang, B. Wang, Y. Yao, and Q. Niu, Phys. Rev. B **84**, 035431 (2011).
[14] G. Z. Magda, X. Jin, I. Hagymási, P. Vancsó, Z. Osváth, P. Nemes-Incze, C. Hwang, L. P. Biró, and L. Tapasztó, Nature (London) **514**, 608 (2014).
[15] J. Jung and A. H. MacDonald, Phys. Rev. B **79**, 235433 (2009).
[16] H. Lee, Y.-W. Son, N. Park, S. Han, and J. Yu, Phys. Rev. B **72**, 174431 (2005).
[17] Q.-F. Sun and X. C. Xie, Phys. Rev. Lett. **104**, 066805 (2010).
[18] B. S. Kandemir and A. Mogulkoc, Phys. Lett. A **379**, 2120 (2015).
[19] M. Ezawa, J. Phys. Soc. Jpn. **76**, 094701 (2007).
[20] L. F. Huang, G. R. Zhang, X. H. Zheng, P. L. Gong, T. F. Cao, and Z. Zeng, J. Phys.: Condens. Matter **25**, 055304 (2013).
[21] A. A. Shylau and I. V. Zozoulenko, Phys. Rev. B **84**, 075407 (2011).
[22] A. Cresti, G. Grosso, and G. P. Parravicini, Phys. Rev. B **77**, 115408 (2008).
[23] Y. Hancock, A. Uppstu, K. Saloriutta, A. Harju, and M. J. Puska, Phys. Rev. B **81**, 245402 (2010).
[24] http://www.physics.rutgers.edu/pythtb.
[25] C. W. Groth, M. Wimmer, A. R. Akhmerov, and X. Waintal, New J. Phys. **16**, 063065 (2014).
[26] K. Nakada, M. Fujita, G. Dresselhaus, and M. S. Dresselhaus, Phys. Rev. B **54**, 17954 (1996).
[27] A. Rycerz, J. Tworzydło, and C. W. J. Beenakker, Nat. Phys. **3**, 172 (2007).
[28] N. Tombros, C. Jozsa, M. Popinciuc, H. T. Jonkman, and B. J. van Wees, Nature (London) **448**, 571 (2007).
[29] R. V. Gorbachev, J. C. W. Song, G. L. Yu, A. V. Kretinin, F. Withers, Y. Cao, A. Mishchenko, I. V. Grigorieva, K. S. Novoselov, L. S. Levitov, and A. K. Geim, Science **346**, 448 (2014).
[30] W. Yao, S. A. Yang, and Q. Niu, Phys. Rev. Lett. **102**, 096801 (2009).
[31] Y.-T. Zhang, Q.-F. Sun, and X. C. Xie, J. Appl. Phys. **109**, 123718 (2011).
[32] C. L. Kane and E. J. Mele, Phys. Rev. Lett. **95**, 226801 (2005).